Elastographic Measurement of the Area and Volume of Thermal Lesions Resulting from Radiofrequency Ablation: Pathologic Correlation

Tomy Varghese[1]
Udomchai Techavipoo[1,2]
Wu Liu[1]
James A. Zagzebski[1]
Quan Chen[1]
Gary Frank[1]
Fred T. Lee, Jr.[3]

OBJECTIVE. Elastography is a promising tool for visualizing the zone of necrosis in liver tissue resulting from radiofrequency tumor ablation. Because heat-ablated tissues are stiffer than normal untreated tissue, elastography may prove useful for following up patients who undergo radiofrequency ablative therapy. We sought to report the initial evaluations of the reliability of elastography for delineating thermal lesion boundaries in liver tissue by comparing lesion dimensions determined by elastography with the findings at whole-mount pathology.

MATERIALS AND METHODS. Radiofrequency ablation was performed in vitro on liver tissue specimens encased in gelatin phantoms. The imaging plane for elastography was perpendicular to the axis of the radiofrequency electrode so that the ablated region was around the center of the plane. To obtain three-dimensional visualization of thermal lesions, we reconstructed the lesions from multiple elastograms by linearly translating the elastographic scanning plane. Pathology photographs were obtained in the same image plane used for elastography by slicing through the gelatin and tissue phantom using external markers. We used digitized gross pathology photographs obtained at a specified slice thickness to compute the areas and volumes of the lesions. These measurements were then compared to the measurements obtained from the elastograms.

RESULTS. In a sample of 40 thermal lesions, we obtained a correlation between in vitro elastographic and pathologic measurements of $r = 0.9371$ ($p < 0.00001$) for area estimates and $r = 0.979$ ($p < 0.00001$) for volume estimates.

CONCLUSION. We found excellent correlation between the measurements of the dimensions, areas, and volumes of thermal lesions that were based on elastographic images and the measurements that were based on digitized pathologic images. When compared with digitized pathologic measurements, elastographic measurements showed a tendency to slighly underestimate both the areas and volumes of lesions. Nevertheless, elastography is a reliable technique for delineating thermal lesions resulting from radiofrequency ablation.

Techniques of imaging elastic properties of tissue for diagnosis of disease are rapidly gaining attention because they are noninvasive and can provide new information on tissue [1–15]. One of these methods, called elastography, can be used to estimate the local strain corresponding to small, externally applied quasistatic compressions [1–3]. Local tissue displacements are estimated with a normalized time-domain cross-correlation between gated radio frequency echo signals obtained before and after compression of the tissue. The axial gradient of the tissue displacements is used to estimate local tissue strain, and these estimates are displayed as gray-scale sonographic images called elastograms [1–3]. Although elastograms are generally obtained using off-line processing, researchers have found real-time applications for elastography using faster algorithms [14] or using algorithms on clinical sonography scanners [16].

Elastography has recently been shown to be useful in monitoring the impact of ablative therapies on tumors [17–20]. Techniques such as radiofrequency ablation produce protein denaturation because of the elevated tissue temperatures; the elevated temperatures, in turn, induce elevation of the elastic modulus of soft tissue. Temperatures greater than 42°C (107.6°F) are considered potentially lethal, depending on the duration of application [21], and temperatures greater than 60°C (140°F) are associated with uniform tissue necrosis [22]. On elastography, radiofrequency ablation lesions exhibit extremely high contrast compared

Received November 4, 2002; accepted after revision March 18, 2003.

Supported in part by grants from The University of Wisconsin–Madison and by grant R01 CA39224 from the National Institutes of Health.

[1]Department of Medical Physics, The University of Wisconsin–Madison, 1530 Medical Sciences Center, 1300 University Ave., Madison, WI 53706. Address correspondence to T. Varghese.

[2]Department of Electrical Engineering, The University of Wisconsin–Madison, Madison, WI 53706.

[3]Department of Radiology, The University of Wisconsin–Madison, Madison, WI 53706.

AJR 2003;181:701–707

0361–803X/03/1813–701

with the normal, untreated background liver tissue [17, 18]. Early work in other laboratories [17–20] and our own preliminary results [17, 18] suggest that sonographic elastography may be substantially superior to conventional sonography for monitoring radiofrequency ablation lesions.

Conventional transabdominal sonography has been used extensively for guidance and monitoring of radiofrequency ablation of hepatic tumors [23, 24]. However, the zone of necrosis produced by radiofrequency ablation is not easily visualized on sonography because of the intrinsically low contrast between normal and ablated liver tissue and because of artifacts resulting from gas bubble formation and from the generator [23, 25]. Microbubble sonography contrast agents have also been investigated as aids in revealing the zone of necrosis generated after radiofrequency ablation [26]. Because these agents are used to differentiate between perfused and nonperfused tissue, the use of contrast sonography may help in the detection of residual or viable nonablated tumor regions.

MRIs of ablated regions reveal altered signals on both T1- and T2-weighted images [23, 25, 27, 28], with the treated areas devoid of gadolinium enhancement.

Radiologic and pathologic correlations in both experimental and clinical studies have shown that CT and MRI can aid radiologists in predicting the region of coagulation within 2–3 mm [29]. Cha et al. [30] compared the usefulness of CT and sonography as methods of monitoring radiofrequency ablation therapy. These researchers found that on CT, radiofrequency ablation lesions consistently showed lower attenuation than the surrounding liver. On sonography, echogenicity of the lesions varied, with approximately 59% of the lesions being hypoechoic; 25%, hyperechoic; and about 16%, isoechoic [30]. Both unenhanced and contrast-enhanced CT offered better conspicuity and edge detection of radiofrequency ablation lesions and fewer artifacts than did sonography. Unenhanced CT had the closest correlation to pathologic size of the lesions (r = 0.74), followed by contrast-enhanced CT (r = 0.72), and sonography (r = 0.56).

The delineation of the boundary of an ablated region is key to making accurate judgments concerning treated versus untreated regions. Our goal in the work described here was to understand more thoroughly how the boundaries of thermal lesions viewed on elastograms correspond to actual ablated tissue boundaries observed histologically. We compared the widths, heights, areas, and volumes of thermal lesions depicted on elastograms with the same parameters of the lesions measured at gross pathology. We performed our analysis under in vitro conditions to evaluate the feasibility of using elastography for monitoring the thermal lesions generated with radiofrequency ablation.

Materials and Methods

In vitro elastography was performed using the set-up illustrated in Figure 1. To provide a regular surface for external quasistatic compression, we encased specimens of liver tissue measuring approximately 40 × 40 mm and 20 mm thick in 80 × 80 mm gelatin cubes.

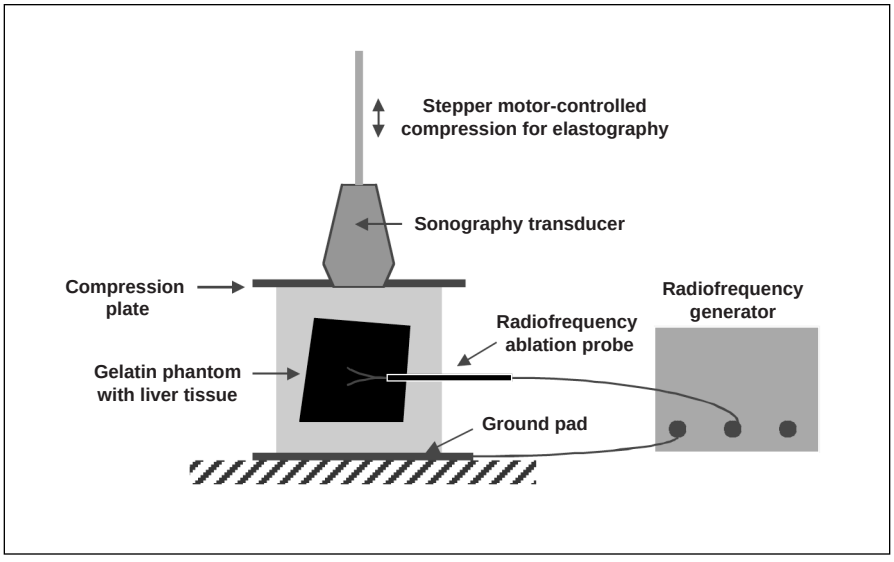

Fig. 1.—Schematic diagram of electrosurgical system (model 1500, RITA Medical Systems, Mountain View, CA) used for radiofrequency ablation elastography. Tips of heating elements in radiofrequency ablation electrode are equipped with thermosensors. Electrode is inserted perpendicular to scanning plane of sonography transducer.

An electrosurgical device (model 1500, RITA Medical Systems, Mountain View, CA) was used for radiofrequency ablation procedures. The radiofrequency ablation electrode in this device consists of a 15-gauge shaft through which multiple sharp tines, each with a diameter of 0.053 cm (0.021 inches; 25 gauge), can be deployed. Fully extended, the tines are in an "umbrella" configuration at 45° intervals. The last 1 cm of the electrode tip and each tine constitute the electrically active surface. We inserted the electrode into the liver lobe and deployed the tines, taking care to keep them within the liver parenchyma. Radiofrequency ablation of the targeted tissue was conducted for 10 min by heating the tissue to set temperatures of 70°, 80°, 90°, or 100°C (158°, 176°, 194°, 212°F), using a 150-W power level.

Freshly excised porcine livers obtained from an adjoining laboratory were used for the analysis. In our initial set of experiments, the thermal lesions were created after normal sections of liver tissue were encased in gelatin. However, ablation of liver tissue inside the gelatin blocks caused some melting of the gelatin, which may have changed the stiffness properties. To avoid this occurrence, we performed radiofrequency ablation on whole liver samples before encasing them in gelatin blocks. Ablation was performed in three to five sections of each liver sample by inserting the radiofrequency ablation electrode about 2–4 cm deep and then switching on the power. After the lesion had cooled, the lesion and the surrounding tissue were encased in a gelatin block for subsequent imaging.

Gelatin phantoms were prepared using 200-bloom calfskin gelatin at a concentration of 15.4 g/L of distilled water. The gelatin powder was mixed with distilled water and cooked in a double-heated water bath to a temperature of 80°C (194°F). After the gelatin solution clarified, glass beads (mean diameter, 8 μm) were mixed with warm distilled water and added to the molten gelatin at a concentration of 1 g of beads per liter of gelatin to provide a source of scattered echo signals during sonography. The molten gelatin was then poured into plexiglass molds. First, a 2.5-cm thick layer of molten gelatin with a temperature of 29°C (82.4°F) was poured. After this layer congealed, we placed a section of liver with a radiofrequency ablation lesion on the gelatin layer. The mold was then filled with molten gel (temperature, 29°C or 82.4°F), and the entire phantom was allowed to congeal for 1 hr. The molds containing the gelatin blocks were refrigerated at 10°C (50°F) for 2 hr. Samples were then removed from the molds for elastography.

We used a real-time scanner (SSD 2000, Aloka, Tokyo, Japan) for elastographic imaging of the thermal lesion, with a 40-mm-wide 5.0-MHz linear array transducer and a 70% bandwidth. In addition, we obtained elastograms using a 3.5-MHz sector transducer to assess the use of lower frequency probes. The raw sonographic radiofrequency echo signals from com-

plete B-mode frames were digitized using a 12-bit data acquisition board (Gage, Montreal, QC, Canada) at a sampling rate of 50 MHz. The apparatus includes a stepper motor–controlled motion-compression system and a compression plate that also supports the transducer. Both the transducer and compression plate were placed in direct contact with the gelatin block. A personal computer was used to control the operation of the system. Elastograms were generated using compressive increments of 0.5%. Signal processing was performed off-line. We computed tissue displacements with time-domain cross-correlation analysis using a 3-mm window length setting, with a 50% overlap between data segments. Elastograms were then obtained using a gradient operator on the estimates of tissue displacement.

Results

Typical in vitro elastograms, sonographic B-mode images, and digitized pathology photographs in both sector and linear formats of the thermal lesions in the excised liver tissue are shown in Figures 2 and 3. The sector images in Figure 2 were obtained using a transducer with a 3.5-MHz center frequency, whereas the linear images in Figure 3 were obtained using a transducer with a 5-MHz center frequency. We believe that these images illustrate that elastography can be performed in either format and over the range of center frequencies used for clinical imaging of the human liver.

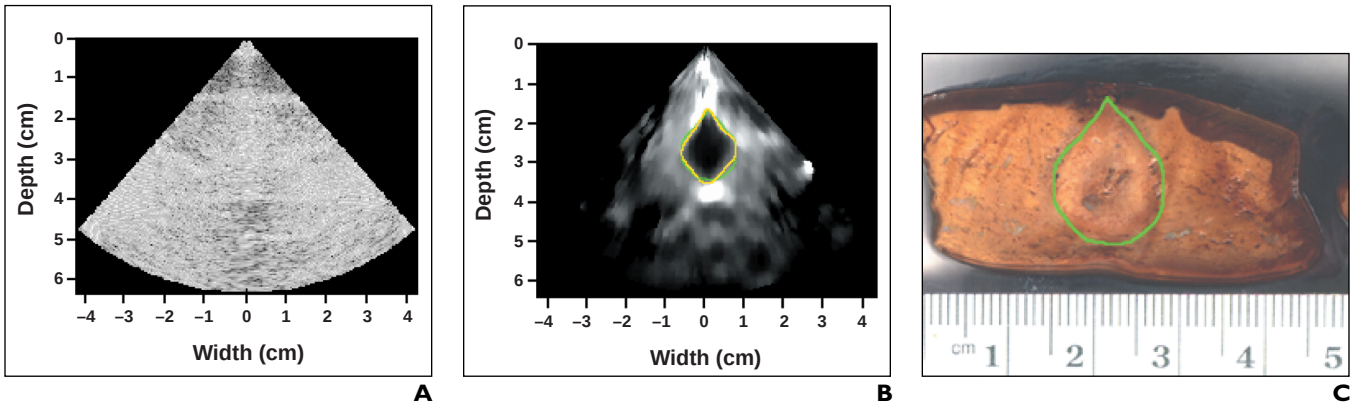

Fig. 2.—Images of radiofrequency ablation thermal lesion in section of liver tissue encased in gelatin phantom. Sonographic images were obtained with 3.5-MHz sector transducer.
A, Sector B-mode gray-scale sonogram of area treated with radiofrequency ablation. Lesion is difficult to see.
B, Two-dimensional elastogram of lesion shows contour of ablated area (*yellow outline*).
C, In digitized photograph of gross pathology specimen, contour of lesion is outlined in green.

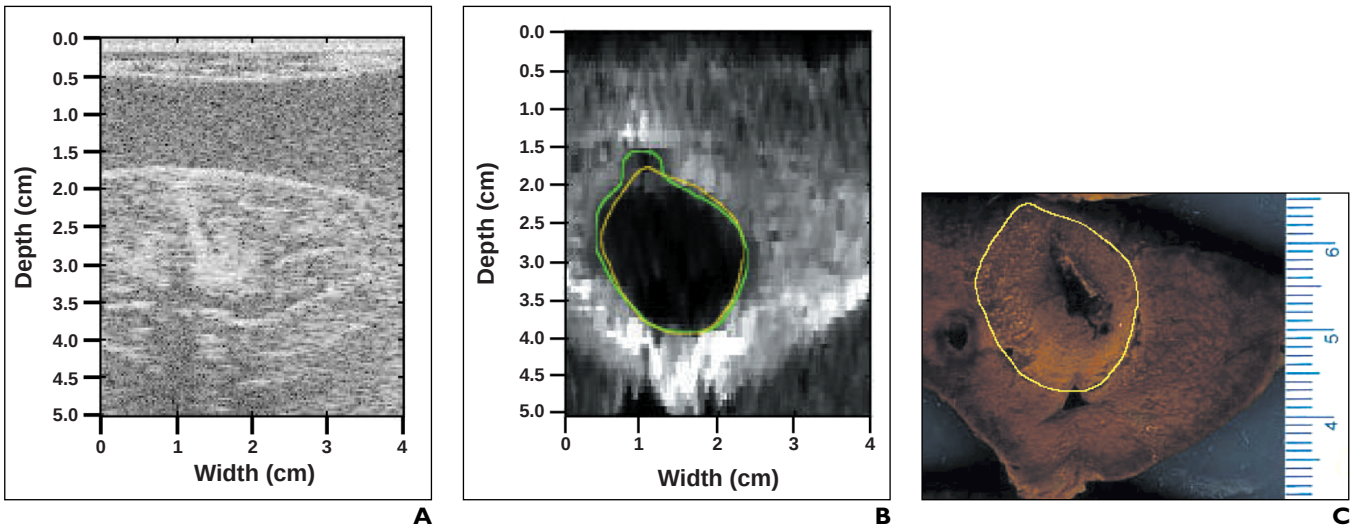

Fig. 3.—Radiofrequency ablation thermal lesion in lobe of liver tissue encased in gelatin phantom. Sonographic images were obtained with 5-MHz linear transducer.
A, Linear B-mode gray-scale sonogram shows increased echogenicity near apparent ablation site and some shadowing below region of high echogenicity. However, distinguishing boundaries (size and position) of thermal lesion is still difficult on conventional sonogram.
B, On axial two-dimensional (2D) elastogram, thermal lesion (*green outline*) is clearly delineated from surrounding tissue. Yellow contour is overlay of lesion area as outlined in **C**.
C, Axial digitized photograph of lesion area (*yellow contour*) in gross pathology specimen from which elastogram (**B**) was generated compares well with area of lesion (*green contour*, **B**) in elastogram. Areas on top (1.5 cm) and bottom (0.5 cm) of elastogram correspond to gelatin, which is slightly stiffer (low-strain regions appear darker) than normal liver tissue. Note close correspondence between lesion as depicted in pathologic specimen photograph and on elastogram, including notch in 11-o'clock position visible on both images.
(Fig. 3. continues on next page)

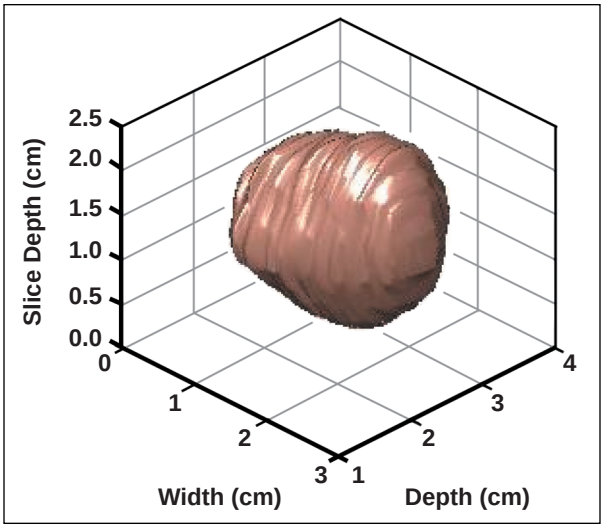

D

Fig. 3. (continued)—Radiofrequency ablation thermal lesion in lobe of liver tissue encased in gelatin phantom. Sonographic images were acquired with 5-MHz linear transducer. **D,** Three-dimensional (3D) elastogram of thermal lesion was produced by reconstructing lesion from multiple 1-mm 2D elastograms obtained along parallel scanning planes. Surface and volume rendering of lesion is possible because of marked contrast in stiffness between lesion and surrounding normal tissue. To render lesion surface, we segmented 2D elastograms by setting a single threshold (strain value 90% below maximum strain surrounding thermal lesion) to separate background strains from lower strains in thermal lesion. With 3D representation, lesion volume can be calculated.

A three-dimensional (3D) visualization of a thermal lesion was generated from parallel, multislice elastograms acquired at 1-mm increments (Fig. 3D). Segmentation of the two-dimensional (2D) elastograms to obtain the lesion surface was performed by setting a single threshold (a strain value 90% below the maximum strain surrounding the thermal lesion) to separate the background strains from the lower strains in the thermal lesion. The 3D representation allows computation of the lesion volume.

Thermal lesion dimensions, areas, and volumes were estimated for 40 thermal lesions to analyze correspondence between elastographic and visual pathologic depictions. Ten sets of in vitro thermal lesions (a set consists of four lesions generated at temperatures of 70°, 80°, 90°, and 100°C or (158°, 176°, 194°, and 212°F) were studied using elastography and compared with corresponding digitized photographs of gross pathology specimens that were sliced along the central sonographic and elastographic scanning planes. Fiducial markers were inscribed on these planes of the gelatin phantom to align both data sets.

Scatterplots of the lesion dimensions (width and height) are presented in Figures 4 and 5, respectively. As these scatterplots

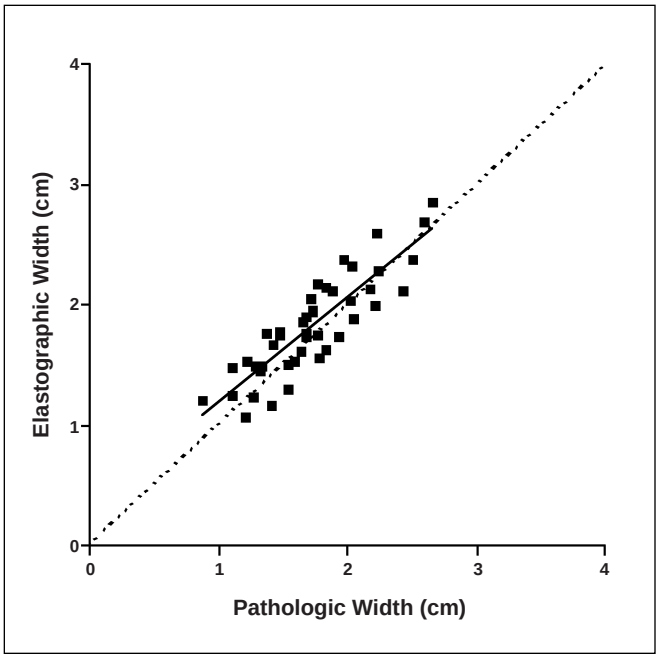

Fig. 4.—Scatterplot of lesion widths at center planes between pathology and elastography and their linear fits. Mean square error is 0.0515. Dotted line at 45° denotes perfect fit between elastographically and pathologically derived areas of lesions, whereas solid line denotes best linear fit of data. Note that lesion widths obtained using elastography closely correspond to widths of thermal lesions observed on pathology specimen, with *r* value of 0.8693.

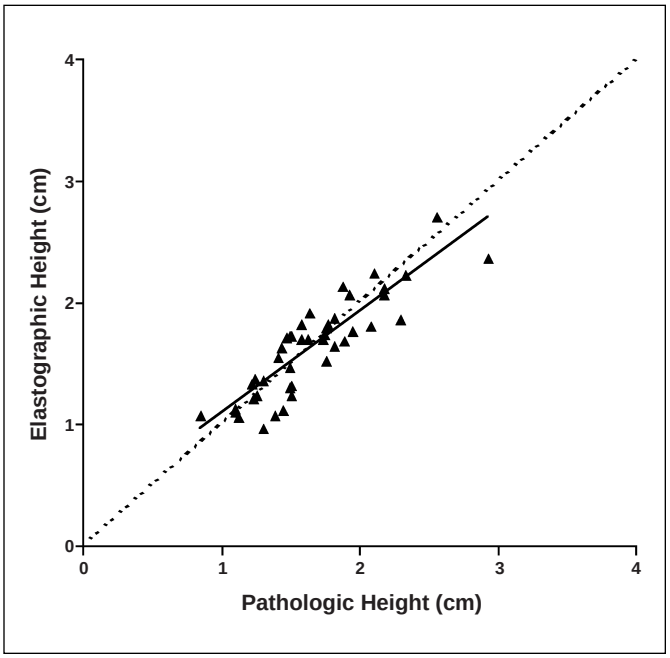

Fig. 5.—Scatterplot of lesion heights at center planes between pathology and elastography and their linear fits. Mean square error is 0.0420. Dotted line at 45° denotes perfect fit between elastographically and pathologically derived heights of lesions, whereas solid line denotes best linear fit of data. Pathologic and elastrographic heights show slightly better correlation ($r = 0.8742$) than was found in lesion widths, implying better fit between data sets for heights than those for widths (Fig. 4).

show, we found that the lesion widths obtained using elastography corresponded closely to the width of the thermal lesion on the digitized photographs of pathology specimens (r = 0.8693). The heights of the lesions on elastograms had a slightly better correspondence to measurements obtained from the pathologic specimens (r = 0.8742), implying a better fit between the data sets. This result is probably explained by the fact that lesion heights were measured in the axial direction, which provides the best sonographic and elastographic resolution. We obtained the areas of the thermal lesion from the width and height measurements so that we could compute the area of the bounding ellipse (Fig. 6), where the r value obtained was 0.9126. However, obtaining areas in this manner does not take into account the errors that may be caused by the shift in the angle that the thermal lesion makes along the principal axes.

Better estimates of the lesion areas were obtained by drawing contours of the lesion shape (including the angle produced by the thermal lesion with the principal axes) and then computing the area of the bounding ellipse. The areas of lesions obtained from the pathology specimens were measured by drawing contours (yellow outline in Figure 3C) that contained only the white zone (region of complete necrosis) of the thermal lesion from the optically scanned images of the gross pathology specimens. The area calculations for elastograms were obtained by drawing a contour (green outline in Figure 3B) that contained only the apparent thermal lesion (i.e., inside the black or stiffer region). Correlation between estimates of areas obtained from elastography and those obtained from pathology specimens improved (r = 0.9371) using this method (Fig. 7). The areas obtained using elastography slightly underestimated the lesion areas. Compared with the best correlation (r = 0.74) reported by Cha et al. [30] between pathologic and unenhanced CT measurements of lesion sizes, our results were significantly better.

Volume estimates for the lesions in gross pathology specimens (Fig. 8) were calculated from a sum of the product of the areas of the thermal lesions multiplied by the thickness of the thermal lesions section, sliced in 1-mm increments. The elastographic lesion volumes were calculated as the sum of the product of the areas obtained from 2D elastograms multiplied by the scanning plane separation of 1 mm. The r value between elastographic and pathologic volumes was 0.979. As we found in the estimates of thermal lesion areas, we discovered an apparent underestimation of the volumes using elastography. The underestimation of the lesion areas and volume using elastography may be an accurate reflection of the underlying stiffness changes, but we plan to investigate this result more extensively.

Discussion

Using elastography to visualize the necrotic zone by imaging the stiffness of treated tissue after radiofrequency ablation has been studied previously [17, 18]. The results of our study prove that elastographic depiction of thermal lesions agrees closely with the results obtained by measuring the lesions in gross pathology specimens and that sonographic elastography potentially may be used to clearly visualize a thermal lesion and to obtain quantitative estimates of its size, area, and volume.

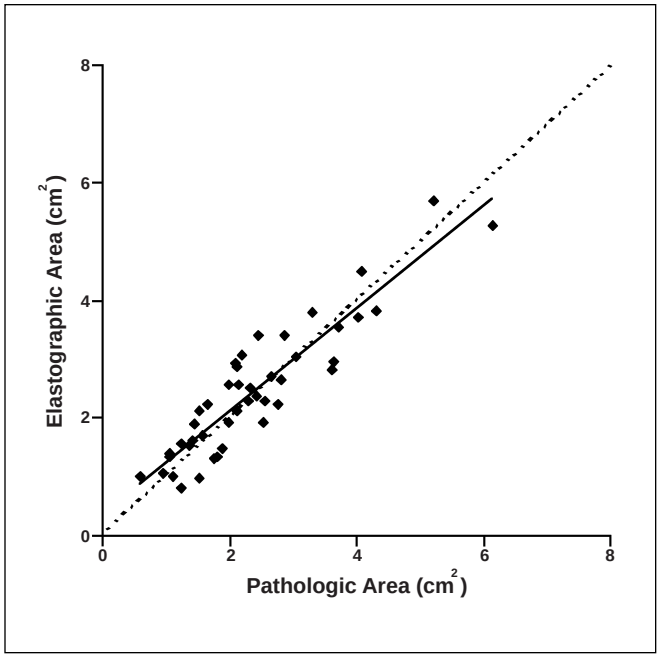

Fig. 6.— Scatterplot of bounding ellipse areas of lesions at center planes between pathology and elastography. Dotted line at 45° denotes perfect fit between elastographically and pathologically derived bounding ellipse areas of lesions, whereas solid line denotes best linear fit of data. Areas were computed using width and depth data; correlation was r = 0.9126. Note that areas obtained using width and depth data do not take into account errors that may be caused by shift in angle of thermal lesion along principal axes.

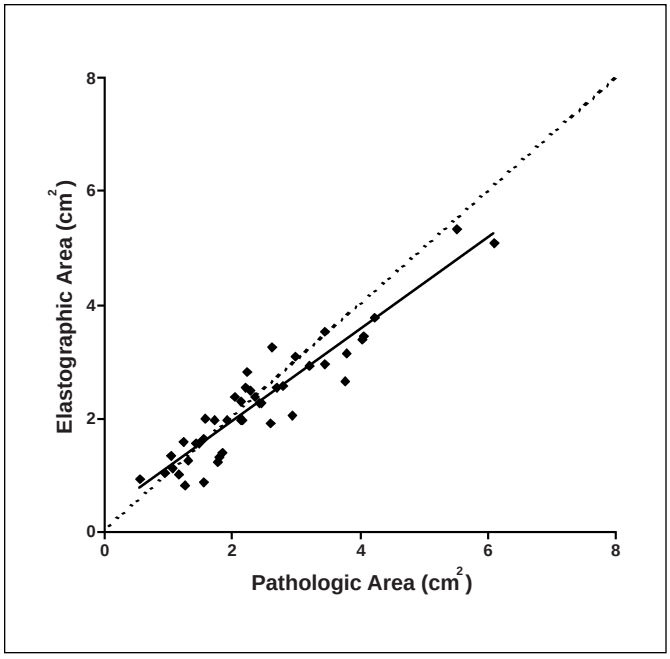

Fig. 7.— Scatterplot compares lesion areas obtained with elastography with areas obtained from gross pathology specimens along center planes. Dotted line at 45° denotes perfect fit between elastographically and pathologically derived areas of lesions, whereas solid line denotes best linear fit of data. Scatterplot and linear fit were obtained over 40 independent data sets. Mean square error is 0.1961.

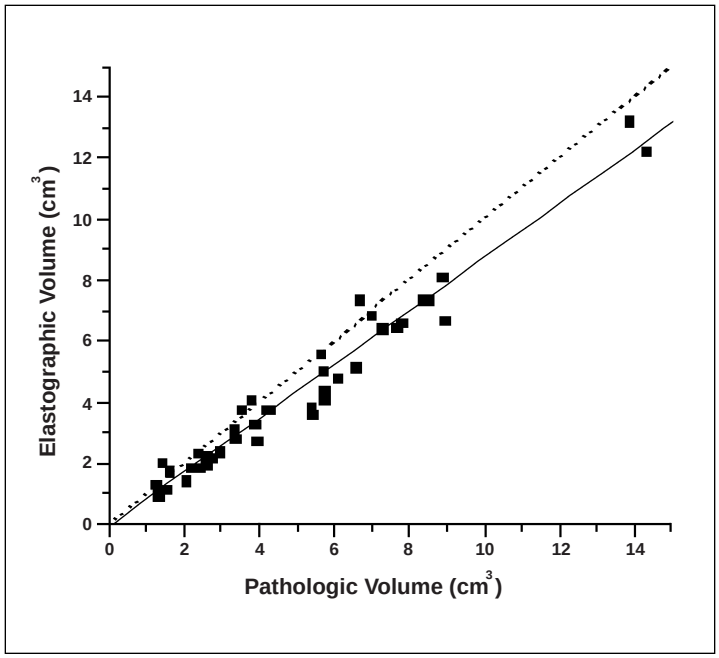

Fig. 8.—Scatterplot compares elastographic measurement of lesion volumes with gross pathologic measurement. Dotted line at 45° denotes perfect fit between elastographically and pathologically derived volumes of lesions, whereas solid line indicates linear fit of data. Scatterplot and linear fit were obtained over 40 independent data sets. Mean square error is 0.11.

In our statistical results, the *r* value between elastographic lesion areas and pathologic lesion areas was approximately 0.93. The comparison with elastographic and pathologic volumes provided higher correlations (r = 0.97). These findings indicate that elastography is potentially a viable technique for delineating thermal lesions.

As a result of this finding, clinicians may be able to assess the success of the procedure or the need to perform additional ablation immediately, as opposed to waiting for a few days to obtain CT scans. In contrast to conventional sonography, 3D surface and volume rendering of thermal lesions generated from elastographic images is made possible by the marked contrast in stiffness between the lesion and the surrounding normal tissue. Imaging of the thermal lesion in 3D also allows computation of the lesion volume, size, and position within the treated region, parameters that indicate the success or failure of the procedure. Although the diameters of thermal lesions imaged in our study were 1–3 cm, the elastograms obtained using the sector probe and the 3.5-MHz center frequency showed that larger and deeper lesions can also be monitored with elastography.

For our analysis, we used in vitro samples in which the controlled quasistatic compressions required for elastography can be easily applied. The feasibility of using in vivo elastography to image radiofrequency-ablated lesions in the liver has already been shown [17, 18]. The use of the radiofrequency ablation electrode as the compressor–displacement device reduces the lateral slippage or nonaxial motion that may occur with externally applied compressions or imaging during the respiratory cycle [17, 18]. This technique provides controlled and reproducible compressions of the liver for in vivo elastography. A complete statistical analysis in a study using in vivo thermal lesions would confirm the usefulness of elastography in monitoring radiofrequency ablation procedures and will be the subject of future research.

Acknowledgments

We thank Larry Whitesell and Jennifer Buck for providing liver tissue samples used for the experiments.

References

1. Ophir J, Cespedes I, Ponnekanti H, Yazdi Y, Li X. Elastography: a quantitative method for imaging the elasticity of biological tissues. *Ultrason Imaging* 1991;2:111–134
2. Cespedes EI. *Elastography: imaging of biological tissue elasticity.* Houston: Univ. of Houston Press, 1993
3. Varghese T, Ophir J, Konofagou E, Kallel F, Righetti R. Tradeoffs in elastographic imaging. *Ultrason Imaging* 2001;4:216–248
4. O'Donnell M, Skovoroda AR, Shapo BM, Emelianov SY. Internal displacement and strain imaging using ultrasonic speckle tracking. *IEEE Trans Ultrason Ferroelectr Freq Control* 1994;41:314–325
5. Doyley MM, Bamber JC, Fuechsel F, Bush NL. A freehand elastographic imaging approach for clinical breast imaging: system development and performance evaluation. *Ultrasound Med Biol* 2001;27:1347–1357
6. Parker KJ, Huang SR, Musulin RA, Lerner RM. Tissue response to mechanical vibrations for "sonoelasticity imaging." *Ultrasound Med Biol* 1990; 16:241–246
7. Maurice RL, Bertrand M. Lagrangian speckle model and tissue-motion estimation: theory. *IEEE Trans Med Imaging* 1999;18:593–560
8. Krouskop TA, Dougherty DR, Vinson FS. A pulsed Doppler ultrasonic system for making noninvasive measurements of the mechanical properties of soft tissue. *J Rehabil Res Dev* 1987; 24:1–8
9. Chen EJ, Novakofski J, Jenkins WK, O'Brien WDJ. Young's modulus measurements of soft tissues with application to elasticity imaging. *IEEE Trans Ultrason Ferroelectr Freq Control* 1996; 43:191–194
10. van der Steen AF, de Korte CL, Cespedes EI. Intravascular ultrasound elastography. *Ultraschall Med* 1998;19:196–201
11. Insana MF, Cook LT, Bilgen M, et al. Maximum-likelihood approach to strain imaging using ultrasound. *J Acoust Soc Am* 2000;107:1421–1434
12. Muthupillai R, Lomas DJ, Rossman PJ, et al. Magnetic resonance elastography by direct visualization of propagating acoustic strain waves. *Science* 1995;269:1854–1857
13. Nightingale K, Soo MS, Nightingale R, Trahey G. Acoustic radiation force impulse imaging: in vivo demonstration of clinical feasibility. *Ultrasound Med Biol* 2002;28:227–235
14. Pesavento A, Lorenz A, Siebers S, Ermert H. New real-time strain imaging concepts using diagnostic ultrasound. *Phys Med Biol* 2000;45:1423–1435
15. Plewes DB, Bishop J, Samani A, Sciarretta J. Visualization and quantification of breast cancer biomechanical properties with magnetic resonance elastography. *Phys Med Biol* 2000;45:1591–1610
16. Zhu Y, Hall TJ. A modified block matching method for real-time freehand strain imaging. *Ultrason Imaging* 2002;3:161–176
17. Varghese T, Zagzebski JA, Techavipoo U, Chen Q, inventors. WARF University of Wisconsin-Madison, assignee. *Elastographic imaging of in-vivo soft tissue.* Pending U.S. patent P02 153US. Washington, DC: U.S. Patent Office
18. Varghese T, Zagzebski JA, Lee FT. Elastographic imaging of thermal lesions in the liver in vivo following radiofrequency ablation: preliminary results. *Ultrasound Med Biol* 2002;28:1467–1473
19. Stafford RJ, Kallel F, Price RE, et al. Elasto-

graphic imaging of thermal lesions in soft tissue: a preliminary study in vitro. *Ultrasound Med Biol* 1998;24:1449–1458

20. Righetti R, Kallel F, Stafford RJ, et al. Elastographic characterization of HIFU-induced lesions in canine livers. *Ultrasound Med Biol* 1999;25: 1099–1113
21. Rosner GL, Clegg ST, Prescott DM, Dewhirst MW. Estimation of cell survival in tumors heated to nonuniform temperature distributions. *Int J Hyperthermia* 1996;12:223–239
22. Zervas NT, Kuwayama A. Pathological characteristics of experimental thermal lesions: comparison of induction heating and radiofrequency electrocoagulation. *J Neurosurg* 1972;37:418–422
23. Solbiati L, Ierace T, Goldberg SN, et al. Percutaneous US-guided radio-frequency tissue ablation of liver metastases: treatment and follow-up in 16 patients. *Radiology* 1997;202:195–203
24. Solbiati L, Goldberg SN, Ierace T, et al. Hepatic metastases: percutaneous radio-frequency ablation with cooled-tip electrodes. *Radiology* 1997; 205:367–373
25. Goldberg SN, Gazelle GS, Solbiati L, et al. Ablation of liver tumors using percutaneous RF therapy. *AJR* 1998;170:1023–1028
26. Solbiati L, Goldberg SN, Ierace T, et al. Radio-frequency ablation of hepatic metastases: postprocedural assessment with a US microbubble contrast agent—early experience. *Radiology* 1999;211: 643–649
27. Hyodoh H, Hyodoh K, Takahashi K, et al. Microwave coagulation therapy on hepatomas: CT and MR appearance after therapy. *J Magn Reson Imaging* 1998;8:451–458
28. Steiner P, Botnar R, Goldberg SN, et al. Monitoring of radio frequency tissue ablation in an interventional magnetic resonance environment: preliminary ex vivo and in vivo results. *Invest Radiol* 1997;32:671–678
29. Goldberg SN, Gazelle GS, Mueller PR. Thermal ablation therapy for focal malignancy: a unified approach to underlying principles, techniques, and diagnostic imaging guidance. *AJR* 2000; 174:323–331
30. Cha CH, Lee FT Jr, Gurney JM, et al. CT versus sonography for monitoring radiofrequency ablation in a porcine liver. *AJR* 2000;175:705–711